has been rationalized for the first time by Kubo and Tomita,[43] who have set up the basis of the theory used to explain the exchange-narrowing phenomenon.[44] When the anisotropic interactions are negligible and the exchange integrals are much larger than the hyperfine constant ($|J_{ij}| \gg |A|$), which is presently the case, the system may be regarded as being approximately in an eigenstate of S^2 and S_z. This leads to the inhomogeneous exchange-narrowing situation described by Ishikawa.[45] The EPR spectra of complex **4** show evidence for the first time of the inhomogeneous exchange-narrowing phenomenon in the powder spectra of an infinite chain of manganese(II) ions antiferromagnetically exchange-coupled through oxalato bridges.

Concluding Remarks

This study points out that croconato bridges are unable to mediate significant spin–spin magnetic exchange interactions between the manganese(II) ions of an infinite chain. In this regard, the behavior of the croconato anion is similar to that of the acetato anion.[6] This study also clearly establishes for the first time that, unlike the croconato dianion or the acetato monoanion, the oxalato dianion is able to mediate small magnetic superexchange interactions between the manganese(II) ions of an infinite chain, of the order of magnitude of those estimated in the case of sulfato bridges.[35] However, at variance with the case of the sulfato-bridged manganese(II) chain, complex **4** and manganese(II) oxalate behave as one-dimensional antiferromagnets.

Supplementary Material Available: Figures 7 and 8, showing the least-squares fit of the experimental molar magnetic susceptibility and effective magnetic moment data per Mn(II) ion to the theoretical equation for isotropic magnetic exchange in a Heisenberg type chain for **1** and **3**, respectively, Tables VII–XIV, listing crystallographic data, hydrogen atom positional parameters, final non-hydrogen atom thermal parameters, deviations of atoms from their least-squares planes, and dihedral angles between these planes for complexes **2** and **4**, respectively, and interatomic distances for the hydrogen-bonded atoms of complex **2**, Tables XVII–XIX, listing the experimental magnetic susceptibility data for complexes **1**, **3**, and **4**, respectively (14 pages); Tables XV and XVI, listing observed and calculated structure factor amplitudes for complexes **2** and **4**, respectively (24 pages). Ordering information is given on any current masthead page.

(43) Kubo, R.; Tomita, K. *J. Phys. Soc. Jpn.* **1954**, *9*, 888–919.
(44) Pake, G. E. In *Paramagnetic Resonance*; Pines, D., Ed.; W. A. Benjamin, Inc.: Reading, MA, 1962; pp 89–95, 140–152.
(45) Ishikawa, Y. *J. Phys. Soc. Jpn.* **1966**, *21*, 1473–1481.

Contribution from the Departments of Chemistry, The Chung-Cheng Institute of Technology, Taiwan, Republic of China, and The University of Mississippi, University, Mississippi 38677

Lower Valence Fluorides of Chromium. 2. The Phase K_xCrF_3 (x = 0.43–0.59)

Y. S. Hong,† K. N. Baker, Jr.,‡ A. V. Shah,‡ R. F. Williamson,‡ and W. O. J. Boo*,‡

Received September 14, 1989

Chemical analyses verify that the composition of K_xCrF_3 ranges from $x = 0.43$ to $x = 0.59$. Three structures were found to coexist within this composition: a $BaTa_2O_6$ type hexagonal structure ($x < 0.50$), a $BaTa_2O_6$ type structure distorted to orthorhombic ($x \approx 0.50$), and a tetragonal tungsten bronze type structure distorted to orthorhombic ($x > 0.50$). From symmetry lowering associated with concomitant ionic ordering, the tetragonal tungsten bronze type structure was deduced to belong to space group C^9_{2v}-*Pba*2.

Introduction

Numerous ternary- and quaternary-phase fluorides of first-row transition metals have been prepared and characterized in this laboratory.[1–6] From careful X-ray diffraction and magnetic measurements on randomly oriented powdered samples, we have concluded that it is the nature of these materials to display various kinds of concomitant ionic ordering at room temperature.

The fluoride systems K_xFeF_3[7] and K_xVF_3[8,9] ($x \approx 0.4$–0.6) were reported to crystallize in the tetragonal tungsten bronze structure. Magnetic measurements made on the vanadium fluoride system support the conclusion that V^{2+} and V^{3+} ions are ordered.[1] This ordering lowers the crystal symmetry from D^5_{4h}-$P4/mbm$ (reported for K_xWO_3[10]) to C^9_{4v}-$P4_2bc$ (reported for $KMnFeF_6$[11]). The K_xCrF_3 system (x = 0.44–0.60), however, was reported by Dumora et al.[12] not to form the tetragonal bronze structure. Instead, a hexagonal structure related to that of $BaTa_2O_6$[13] was formed. Neither variations in the structure of K_xCrF_3 with composition nor evidence of concomitant ionic ordering (such as small crystal distortions or superstructures) was reported; and no mention was made of magnetic measurements. They did, however, report an attempt to prepare single crystals from the melt (850 °C), which produced some monocrystals with hexagonal lattice parameters a = 21.53 Å and c = 7.610 Å.

The reason the tetragonal tungsten bronze structure did not form for K_xCrF_3 was believed to be related to the Jahn–Teller ion, Cr^{2+}, but there may be conditions under which the bronze structure will form. If the tetragonal bronze phase does form, we would expect to observe Jahn–Teller cooperative ordering in addition to ordering of Cr^{2+} and Cr^{3+} ions. This additional order should further lower its crystal symmetry.

We chose to study the K_xCrF_3 phase (x = 0.44–0.60) to determine if ordering phenomena or other composition-dependent properties may exist at room temperature. Our initial characterization (A series) was so surprisingly different from the results of the French authors[12] that we repeated the synthesis (B series).

Experimental Section

Appropriate quantities of KF, CrF_2, and CrF_3 were vacuum-encap-

† The Chung-Cheng Institute of Technology.
‡ The University of Mississippi.

(1) Hong, Y. S.; Williamson, R. F.; Boo, W. O. J. *Inorg. Chem.* **1980**, *19*, 229.
(2) Hong, Y. S.; Williamson, R. F.; Boo, W. O. J. *Inorg. Chem.* **1981**, *20*, 403.
(3) Banks, E.; Shone, M.; Hong, Y. S.; Williamson, R. F.; Boo, W. O. J. *Inorg. Chem.* **1982**, *21*, 3894.
(4) Hong, Y. S.; Williamson, R. F.; Boo, W. O. J. *Inorg. Chem.* **1982**, *21*, 3898.
(5) Hong, Y. S.; Baker, K. N.; Williamson, R. F.; Boo, W. O. J. *Inorg. Chem.* **1984**, *23*, 2787.
(6) Williamson, R. F.; Arafat, E. S.; Baker, K. N.; Rhee, C. H.; Sanders, J. R.; Scheffler, T. B.; Zeidan, H. S.; Boo, W. O. J. *Inorg. Chem.* **1985**, *24*, 482.
(7) dePape, R. *Bull. Soc. Chim. Fr.* **1965**, 3489.
(8) Garrard, B. J.; Wanklyn, B. M.; Smith, S. H. *J. Cryst. Growth* **1974**, *22*, 169.
(9) Cros, C.; Feurer, R.; Pouchard, M.; Hagenmuller, P. *Rev. Chim. Miner.* **1974**, *11*, 585.
(10) Magneli, A. *Ark. Kemi* **1949**, *11*, 213.
(11) Banks, E.; Nakajima, S.; Williams, G. J. B. *Acta Crystallogr.* **1979**, *B35*, 46.
(12) Dumora, D.; Raney, J.; Hagenmuller, P. *Bull. Soc. Chim. Fr.* **1970**, *5*, 1751.
(13) Layden, G. K. *Mater. Res. Bull.* **1968**, *3*, 349.

0020-1669/90/1329-3037$02.50/0

Table I. Chemical Analyses of K_xCrF_3 Compounds (A and B Series)

		%		formula	
sample	element	calcd	found	theoret	exptl
A-K450CRF3	K	13.90	13.81	$K_{0.450}CrF_3$	$K_{0.445}CrF_{2.98}$
	Cr	41.08	41.25		
	F	45.0			
A-K475CRF3	K	14.56	14.39	$K_{0.475}CrF_3$	$K_{0.472}CrF_{3.04}$
	Cr	40.76	40.53		
	F	44.7			
A-K500CRF3	K	15.21	15.21	$K_{0.500}CrF_3$	$K_{0.497}CrF_{2.96}$
	Cr	40.45	40.70		
	F	44.3			
A-K525CRF3	K	15.85	15.65	$K_{0.525}CrF_3$	$K_{0.516}CrF_{2.99}$
	Cr	40.15	40.30		
	F	44.0			
A-K550CRF3	K	16.48	16.24	$K_{0.550}CrF_3$	$K_{0.541}CrF_{3.01}$
	Cr	39.85	39.91		
	F	43.7			
A-K575CRF3	K	17.10	16.99	$K_{0.575}CrF_3$	$K_{0.569}CrF_{2.98}$
	Cr	39.55	39.73		
	F	43.4			
A-K600CRF3	K	17.71	17.59	$K_{0.600}CrF_3$	$K_{0.593}CrF_{2.98}$
	Cr	39.26	39.45		
	F	43.0			
B-K4625CRF3	K	13.57	13.45	$K_{0.4625}CrF_3$	$K_{0.456}CrF_{3.04}$
	Cr	40.92	40.78		
	F	44.85			
B-K4875CRF3	K	14.88	14.93	$K_{0.4875}CrF_3$	$K_{0.490}CrF_{3.01}$
	Cr	40.61	40.53		
	F	44.51			
B-K5125CRF3	K	15.53	15.36	$K_{0.5125}CrF_3$	$K_{0.510}CrF_{3.05}$
	Cr	40.30	40.07		
	F	44.17			
B-K5375CRF3	K	16.16	15.83	$K_{0.5375}CrF_3$	$K_{0.520}CrF_{2.98}$
	Cr	39.99	40.50		
	F	43.84			
B-K5625CRF3	K	16.79	16.27	$K_{0.5625}CrF_3$	$K_{0.542}CrF_{3.00}$
	Cr	39.70	39.92		
	F	43.51			
B-K5875CRF3	K	17.41	17.32	$K_{0.5875}CrF_3$	$K_{0.580}CrF_{2.96}$
	Cr	39.40	39.74		
	F	43.19			

sulated inside 1.91 cm diameter by 3.18 cm length molybdenum containers by means of electron-beam welding techniques. The A series compounds were heated for 28 days at 850 °C, and the B series compounds were heated for 21 days at 800 °C. Both series were cooled at the rate of 100° h^{-1}. Products were analyzed optically by stereoscopic and polarized microscopy. Chemical analyses were performed by Galbraith Laboratories. Potassium and chromium were determined by atomic absorption (±2%), and fluorine was estimated by difference. Samples were characterized by Guinier-Hagg X-ray techniques using Cu $K\alpha_1$ and Cr $K\alpha_1$ radiations. Magnetic measurements were made from 4.2 to 300 K between 0.14 and 10 kG with a Foner-type PAR vibrating-sample magnetometer equipped with a Janis liquid-helium Dewar flask and a gallium arsenide temperature controller. Magnetic fields were measured with an F. W. Bell hall-probe gaussmeter, Model 8860. Magnetic data were corrected for core diamagnetism from ionic susceptibility tables by Mulay.[14]

Results

All of the series A and B products consisted of dense polycrystalline material. The transmitted color of the K_xCrF_3 compounds is bright green. The color and optical density at each composition appear to be the sum of CrF_3 (light green) and CrF_2 (greenish blue), from which the samples were prepared. The birefringence of K_xCrF_3, when viewed between crossed Nicol prisms, is moderately strong over the entire composition span, with only a slight decrease in samples of low x (0.475 and below). Considerable amounts of a phase of lower optical density were found in samples of composition x below 0.44, and a small amount of an isotropic phase was present in samples of composition x above 0.58. Chemical analyses of samples from the A and B series above $x = 0.44$ are shown in Table I.

(14) Mulay, L. N. *Magnetic Susceptibility*; Interscience: New York, 1963; p 1782.

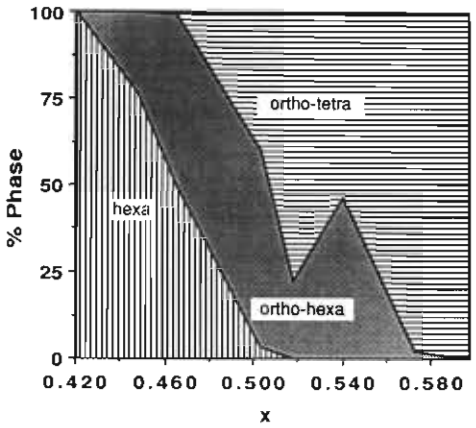

Figure 1. Phase relations as a function of x (A series).

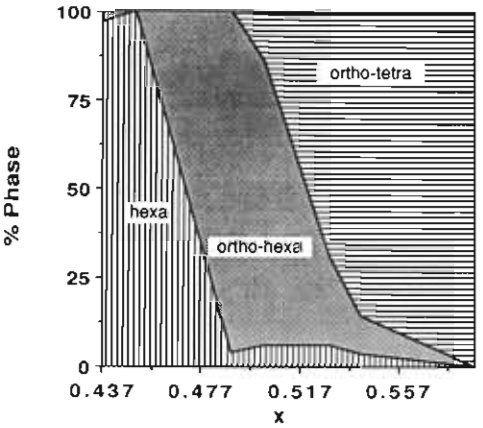

Figure 2. Phase relations as a function of x (B series).

X-ray Diffraction. The low-angle, Guinier-Hagg X-ray data of the B series using Cr $K\alpha_1$ radiation are given in Table II. As in past publications,[2,5] the symbols S = strong, M = medium, W = weak, W^{-1} = very weak, etc. are observable relative intensities. These data were fitted to three crystal structures: a hexagonal structure ($a = 21.5$ Å, $c = 7.6$ Å), a hexagonal structure distorted slightly to orthorhombic ($a = 36.8$ Å, $b = 21.6$ Å, $c = 7.5$ Å), and a tetragonal structure distorted slightly to orthorhombic ($a = 13.1$ Å, $b = 12.5$ Å, $c = 7.8$ Å). Estimates of the relative amounts of each structure were made from the intensities of the (002) and (004) reflections of the three structures within each sample. Figure 1 is a plot of the phase relations as a function of x found in the A series. Figure 2 is a similar plot of the B series. Samples below $x = 0.46$ consist primarily of the hexagonal structure, and samples above $x = 0.54$ are essentially pure pseudotetragonal. All of the other samples are a mixture of two or three structures, although those samples in which x is close to 0.50 are mostly pseudohexagonal. Precise lattice dimensions of the three structures found in the B series are shown in Table III.

Distortion ratios for the pseudohexagonal unit cell and for the pseudotetragonal unit cell are also included in Table III. For the pseudohexagonal unit cell, the distortion ratio is defined as $a/(\sqrt{3}b)$; for the pseudotetragonal unit cell, it is simply a/b.

Magnetic Susceptibilities. Figure 3 is a plot of the magnetic susceptibility, plus a constant (α), versus temperature for each of the samples from the B series. The constant (α), which has no physical significance, is added to separate the data for the different samples. No ferromagnetic components were observed for any of the samples. The magnetic constants C_M, Θ, and T_N are summarized in Table IV. The observed C_M values were calculated from susceptibility data above 150 K. The calculated values of C_M were obtained from the equation in which the previously calculated values $C_{2+} = 3.00$ and $C_{3+} = 1.88$ were used.[5]

$$C_M = xC_{2+} + (1 - x)C_{3+}$$

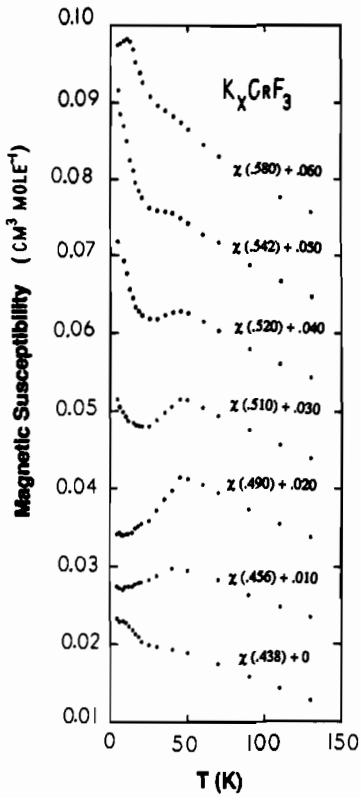

Figure 3. Magnetic susceptibility, plus a constant (α), versus temperature for each of the samples of the B series.

Discussion

The chemical analyses indicate that the composition x ranges from 0.43 to 0.59. X-ray diffraction data reveal that a continuum of phases exists in that composition span and that three distinct structures are present (Figures 1 and 2). A hexagonal structure ($BaTa_2O_6$ type) exists in the range $x = 0.43$–0.50. A distortion of the hexagonal $BaTa_2O_6$ type structure to orthorhombic symmetry was also characterized. Although the distorted structure is optimum near $x = 0.50$, it was found to be present in lesser amounts over most of the composition span. In the range $x \approx 0.50$–0.59 there exists a third structure (also orthorhombic) that appears to be a distortion of the tetragonal tungsten bronze structure. The chemical analyses for both the A and B series agree with the nominal composition within a few percent. Figures 1 and 2, however, show some minor discrepancies in phase composition. It is likely that some segregation of phases occurred in the A series, since it was heated near melting temperature.

Superlattice structures and/or small crystal distortions are often an indication of ionic ordering. In some cases, magnetic properties also support ionic ordering phenomena. In Figure 3, samples of composition $x = 0.520$, 0.510, 0.490, and 0.456 display maxima in magnetic susceptibility near 50 K, and all other samples indicate the presence of a shoulder at this temperature. The sample of composition $x = 0.580$ shows a maximum at 10 K and samples of composition $x = 0.542$, 0.520, and 0.510 each indicate a rise in magnetic susceptibility below 50 K. These effects support the existence of the three phases illustrated in Figures 1 and 2. We conclude that the magnetic susceptibility of the hexagonal $BaTa_2O_6$ phase ($x = 0.438$) has no distinct maximum; the maximum at 50 K is associated with the orthorhombically distorted hexagonal phase, and the maximum at 10 K is associated with the distorted tetragonal tungsten bronze phase. Other than the fact that each of the three distinct phases in the K_xCrF_3 system has a characteristic magnetic susceptibility, no conclusions regarding ionic ordering have been drawn from the magnetic data.

Since the K_xCrF_3 compounds contain Cr^{2+} in octahedral coordination, we expect to see considerable distortion as a consequence of Jahn–Teller cooperative ordering. In the tetragonal tungsten bronze type structure there is obvious distortion in the *ab* plane, causing *a* to be greater than *b* by about 4% (distortion ratios ~ 1.044). The hexagonal $BaTa_2O_6$ structure appears to become ordered at $x = 0.50$. Again, a distortion in the *ab* plane is apparent from the distortion ratios (~0.985). This distortion is of the order of 1.5%. All three structures are layer structures. The composition of the layers should be CrF_2, and that of the interlayers K_xF. Since all three structures have this same layer and interlayer composition, small differences in the interlayer distances may provide additional clues as to the orientation of the Jahn–Teller ion, Cr^{2+}. Figure 4 is a plot of the interlayer distances of the three structures in each of the samples. This plot dramatically illustrates that the interlayer distance in the pseudotetragonal structure is 3–4% greater than that in the hexagonal or pseudohexagonal structures. These data support the conclusion that Jahn–Teller distortion in the pseudohexagonal phase occurs only in the *ab* plane, and if the Cr^{2+} ions are elongated, they probably do not have collinear local axes. The pseudotetragonal phase appears to increase in both *a* (~4%) and *c* (~3–4%). In a distorted tetragonal tungsten bronze structure, however, the Cr^{2+} ions probably occupy three different lattice sites, and the data suggest their local axes are not collinear either.

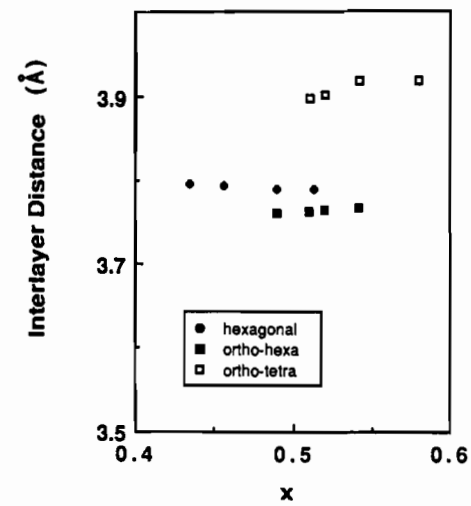

Figure 4. Plot of the interlayer distances of the three structures in each sample.

The lowering of symmetry of the tetragonal tungsten bronze structure to orthorhombic provides an interesting example of the relationship between symmetry and ordering phenomena. In previous studies,[1,3] we concluded that first-row transition-metal analogues of tetragonal tungsten bronze, $K_xM^{II}{}_xM^{III}{}_{1-x}F_3$, display M^{2+}–M^{3+} ionic ordering. This ordering lowers the space group symmetry from D^5_{4h}-$P4/mbm$ to C^8_{4v}-$P4_2bc$. In the tetragonal tungsten bronze structure of $K_xCr^{II}{}_xCr^{III}{}_{1-x}F_3$ ($x \sim 0.50$–0.59), we assume that Cr^{2+}–Cr^{3+} ordering occurs. In addition, cooperative Jahn–Teller ordering further lowers the symmetry from tetragonal to orthorhombic. We believe this concomitant ordering occurs as solid–solid phase transitions at temperatures below melting but above ambient. It is reasonable to assume that Cr^{2+}–Cr^{3+} ordering occurs first, since the Jahn–Teller ion (Cr^{2+} in its ground state) is undefined above the Cr^{2+}–Cr^{3+}-ordering temperature. Ordering phenomena of this kind can be thought of as imposing an additional pattern on the existing structure. What this means is simply that each new ordered pattern will probably lower the symmetry of the crystal. By examining the subgroups of a known space group, it is often possible to correctly predict the space group of the more ordered structure. From the maximum subgroups of C^8_{4v}-$P4_2bc$, only two are orthorhombic, C^8_{2v}-$Pba2$ and C^{13}_{2v}-$Ccc2$.[15] The reflection conditions hkl ($h + k = 2n$) and $hk0$ ($h + k = 2n$) rule out the second space group, leaving C^8_{2v}-$Pba2$ as the unique choice. The subgroup routing of the tetragonal bronze phase as concomitant ordering sets in is illustrated in Figure 5. From this diagram, we surmise that

(15) *International Tables for X-ray Crystallography*; Hahn, T., Ed.; D. Reidel Publishing Co.: Dordrecht, Holland, 1987; Vol. A.

Table II. Guinier-Hagg X-ray Data for K_xCrF_3 (B Series) [Cr $K\alpha_1$ Radiation (λ = 2.289 62 Å)]

hexagonal (*hkl*)	pseudohexa (*hkl*)	pseudotetra (*hkl*)	*d*(obsd)/*I*(obsd) *d*(calcd)						
			$K_{0.438}CrF_3$	$K_{0.456}CrF_3$	$K_{0.490}CrF_3$	$K_{0.510}CrF_3$	$K_{0.520}CrF_3$	$K_{0.542}CrF_3$	$K_{0.580}CrF_3$
			6.260/W^{-2}	6.265/W^{-5}	6.285/W^{-4}	6.297/W^{-4}			
(300)			6.220	6.215	6.214	6.218			
						5.846/W^{-6}		5.855/W^{-5}	5.904/W^{-6}
		(210)				5.820		5.824	5.817
						5.689/W^{-6}	5.664/W^{-6}	5.670/W^{-5}	5.729/W^{-6}
		(120)				5.654	5.659	5.659	5.666
			5.384/M	5.379/M	5.395/W^{-}	5.402/W	5.366/W^{-2}	5.349/W^{-4}	
(220)			5.386	5.383	5.381	5.385			
	(040)				5.386	5.383	5.383	5.383	
					5.263/M^{-}	5.266/W	5.266/W^{-2}	5.220/W^{-4}	
	(620)				5.325	5.323	5.326	5.324	
			4.658/W^{-3}	4.665/W^{-2}	4.673/W^{-6}	4.677/W^{-5}			
(400)			4.665	4.662	4.660	4.664			
					4.388/W^{-4}	4.392/W^{-4}	4.387/W^{-6}	4.368/W^{-6}	
	(041)				4.380	4.378	4.379	4.380	
						4.147/W^{-3}	4.137/W^{-4}	4.128/W^{-2}	4.154/W^{-3}
		(310)				4.136	4.140	4.139	4.132
			4.1020W^{-4}	4.099/W^{-4}					
(410)			4.072	4.069					
					4.036/W^{-4}	4.028/W^{-5}	4.024/W^{-6}		
	(640)				4.045	4.043	4.044		
						4.001/W^{-5}	3.982/W^{-4}	3.977/W^{-4}	4.006/W^{-4}
		(130)				3.979	3.983	3.983	3.990
						3.904/W^{-}	3.902/M^{+}	3.929/M^{+}	3.939/S
		(002)				3.898	3.902	3.983	3.919
			3.798/S	3.794/S	3.796/W^{-4}	3.798/W^{-3}	3.794/W^{-3}	3.785/W^{-5}	
(002)			3.796	3.793	3.789	3.789	3.794	3.785	
			3.769/W^{-4}		3.768/S^{-}	3.771/M^{+}	3.762/W^{+}	3.756/W^{-2}	
	(002)		3.769		3.762	3.763	3.766	3.767	
						3.593/W^{-}	3.595/W^{-2}	3.589/W^{-2}	3.603/M^{+}
		(112)				3.581	3.585	3.597	3.598
		(320)				3.590	3.594	3.593	3.590
						3.530/W^{-3}	3.532/W^{-2}	3.526/W^{-2}	3.536/M
		(230)				3.524	3.528	3.528	5.530
			3.331/M^{-}	3.328/W					
(212)			3.342	3.340					
						3.287/W^{-5}	3.290/W^{-5}	3.290/W^{-5}	3.290/W^{-5}
		(400)				3.286	3.289	3.288	3.282
			3.2640W^{-4}	3.263/W^{-2}					
(331)			3.246	3.244					
					3.256/W^{-6}	3.242/W^{-2}	3.242/W^{-4}	3.243/W^{-4}	3.251/W^{-2}
	(061)				3.241	3.239	3.240	3.240	
		(212)			3.252	3.239	3.242	3.251	3.250
					3.229/W^{-4}	3.209/W^{-3}	3.212/W^{-4}	3.213/W^{-4}	3.225/W^{-2}
	(602)				3.206	3.206	3.208	3.209	
		(122)			3.221	3.209	3.212	3.221	3.223
						3.180/W^{-2}	3.182/W^{-4}	3.180/M	3.178/W^{-2}
		(410)				3.179	3.182	3.181	3.175
			3.104/S^{+}	3.107/S^{+}	3.105/W^{-2}	3.108/W^{-3}	3.106/W^{-3}	3.100/W^{-4}	
(600)			3.110	3.108	3.107	3.109			
	(660)				3.098	3.096	3.097	3.097	
					3.085/M^{+}	3.088/M^{+}	3.088/W^{-2}	3.084/W^{-4}	
	(042)				3.084	3.084	3.086	3.086	
			3.058/M	3.058/M^{+}	3.055/S^{+}	3.058/S	3.054/S	3.051/M^{+}	3.052/W^{-2}
(312)			3.061	3.058	3.056	3.057			
	(12,0,0)				3.063	3.062	3.064	3.063	
		(140)				3.046	3.049	3.049	3.054
						3.0240W^{-5}	3.024/W^{-4}	3.025/W^{-3}	3.029/W^{-5}
		(330)				3.023	3.026	3.025	3.025
			2.953/W^{-3}	2.950/W^{-4}					
(402)			2.944	2.942					
							2.961/W^{-3}	2.960/W^{-2}	2.966/W^{-3}

Table II (Continued)

hexagonal (*hkl*)	pseudohexa (*hkl*)	pseudotetra (*hkl*)	d(obsd)/I(obsd) d(calcd) $K_{0.438}CrF_3$	$K_{0.456}CrF_3$	$K_{0.490}CrF_3$	$K_{0.510}CrF_3$	$K_{0.520}CrF_3$	$K_{0.542}CrF_3$	$K_{0.580}CrF_3$
		(222)					2.959	2.966	2.966
		(420)				2.914/W^{-3} 2.910	2.914/W^{-3} 2.913	2.912/W^{-2} 2.912	2.909/W^{-3} 2.909
		(312)				2.837/W^{-3} 2.837	2.841/W^{-2} 2.839	2.842/W^{+} 2.845	2.841/W^{-2} 2.843
		(240)				2.827	2.830	2.830	2.833
		(132)				2.785/W^{-3} 2.787	2.788/W^{-2} 2.793		2.794/W^{-2} 2.796

Table III. Lattice Constants and Distortion Ratios of Three Structures Found in the K_xCrF_3 Phase (B Series)

sample	hexagonal Å	pseudohexa Å	pseudohexa $a/(\sqrt{3}b)$	pseudotetra Å	pseudotetra a/b
$K_{0.438}CrF_3$	a = 12.55 b = 7.592				
$K_{0.456}CrF_3$	a = 21.53 b = 7.586				
$K_{0.490}CrF_3$	a = 21.53 b = 7.577	a = 36.75 b = 21.54 c = 7.524	0.985		
$K_{0.510}CrF_3$	a = 21.54 b = 7.579	a = 36.74 b = 21.53 c = 7.525	0.985	a = 13.145 b = 12.526 c = 7.796	1.049
$K_{0.520}CrF_3$		a = 36.77 b = 21.53 c = 7.531	0.986	a = 13.158 b = 12.537 c = 7.804	1.050
$K_{0.542}CrF_3$		a = 36.75 b = 21.53 c = 7.534	0.985	a = 13.153 b = 12.539 c = 7.836	1.049
$K_{0.580}CrF_3$				a = 13.127 b = 12.563 c = 7.838	1.045

Table IV. Magnetic Constants of the K_xCrF_3 Samples (B Series)

compn	C_M, cm^3 deg mol^{-1} calcd	C_M, cm^3 deg mol^{-1} obsd	Θ, K	T_N, K
$K_{0.438}CrF_3$	2.37	2.67	−78	
$K_{0.456}CrF_3$	2.42	2.83	−84	45
$K_{0.490}CrF_3$	2.43	2.82	−77	50
$K_{0.510}CrF_3$	2.45	2.86	−78	45
$K_{0.520}CrF_3$	2.46	2.95	−77	45
$K_{0.542}CrF_3$	2.49	2.93	−68	
$K_{0.580}CrF_3$	2.53	2.98	−60	10

Cr^{2+}–Cr^{3+} ordering lowers the symmetry from D^5_{4h}-$P4/mbm$ to C^8_{4v}-$P4_2bc$. This process involves two steps: (1) the reduction of translational symmetry (the 4-fold axis becomes a screw axis) and (2) the elimination of the horizontal plane. The two may occur simultaneously, but if not, it is most likely that the formation of the 4-fold screw axis occurs first. Therefore, the correct lowering path should be the one that includes D^{13}_{4h}-$P4_2/mbc$. Finally, cooperative Jahn–Teller ordering of Cr^{2+} lowers the symmetry from C^8_{4v}-$P4_2bc$ to C^8_{2v}-$Pba2$ by eliminating the 4-fold screw axis. This analysis suggests that the tetragonal bronze phase of K_xCrF_3 may have as many as three high-temperature phase transitions below its melting temperature.

Unfortunately, the pseudohexagonal phase does not have a unique space group based on symmetry arguments. One piece of experimental information about the hexagonal phase which is significant is that the c value is doubled. This probably means that the hexagonal phase K_xCrF_3 has some form of Cr^{2+}–Cr^{3+} ordering, whereas the pseudohexagonal phase demonstrates cooperative Jahn–Teller ordering as well.

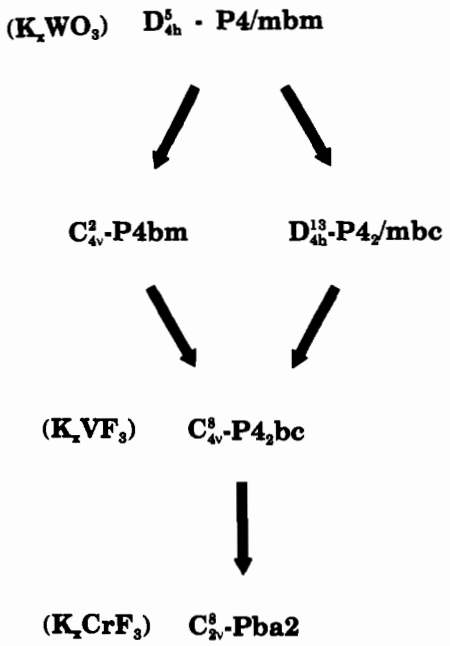

Figure 5. Symmetry lowering of the tetragonal bronze structure.

Conclusions

The K_xCrF_3 phase (x = 0.43–0.56) consists of three distinct structures: a hexagonal structure, a hexagonal structure distorted to orthorhombic, and a tetragonal structure distorted to orthorhombic. The hexagonal structure observed at the lower values of x is of the $BaTa_2O_6$ type and is similar to that reported earlier.[12] The pseudohexagonal structure is an ordered phase which is related to the hexagonal structure. The existence of a tetragonal tungsten bronze related phase containing the Jahn–Teller ion Cr^{2+} was established. The tetragonal tungsten bronze phase demonstrates symmetry lowering as a consequence of Cr^{2+}–Cr^{3+} ordering and cooperative Jahn–Teller ordering. A space group for the pseudotetragonal structure is proposed on the basis of these symmetry arguments.

Acknowledgment. We gratefully acknowledge the National Science Foundation (Grant DMR 79-00313) for financial support and the University of Mississippi for cost sharing. Appreciation is expressed to the University of Mississippi Computer Center for providing data reduction time.